Published in final edited form as:
Cell. 2012 March 2; 148(5): 973–987. doi:10.1016/j.cell.2011.12.034.

Arp2/3 complex is critical for lamellipodia and organization of cell-matrix adhesion but dispensable for fibroblast chemotaxis

Congying Wu[*,1,4], **Sreeja B. Asokan**[*,1,4], **Matthew E. Berginski**[2], **Elizabeth M. Haynes**[1,4], **Norman E. Sharpless**[3,4], **Jack D. Griffith**[4,5], **Shawn M. Gomez**[2], and **James E. Bear**[#,1,4,6]

[1]Dept of Cell & Developmental Biology, University of North Carolina School of Medicine; Chapel Hill, NC 27599 USA

[2]Depts of Biomedical Engineering, Computer Science and Pharmacology, University of North Carolina School of Medicine; Chapel Hill, NC 27599 USA

[3]Dept of Genetics, University of North Carolina School of Medicine; Chapel Hill, NC 27599 USA

[4]Lineberger Comprehensive Cancer Center, University of North Carolina School of Medicine; Chapel Hill, NC 27599 USA

[5]Dept of Biochemistry, University of North Carolina School of Medicine; Chapel Hill, NC 27599 USA

[6]Howard Hughes Medical Institute

SUMMARY

Lamellipodia are sheet-like, leading edge protrusions in firmly adherent cells that contain Arp2/3-generated dendritic actin networks. Although lamellipodia are widely believed to be critical for directional cell motility, this notion has not been rigorously tested. Using fibroblasts derived from Ink4a/Arf-deficient mice, we generated a stable line depleted of Arp2/3 complex that lacks lamellipodia. This line shows defective random cell motility and relies on a filopodia-based protrusion system. Utilizing a microfluidic gradient generation system, we tested the role of Arp2/3 complex and lamellipodia in directional cell migration. Surprisingly, Arp2/3-depleted cells respond normally to shallow gradients of PDGF indicating that lamellipodia are not required for fibroblast chemotaxis. Conversely, these cells cannot respond to a surface-bound gradient of extracellular matrix (haptotaxis). Consistent with this finding, cells depleted of Arp2/3 fail to globally align focal adhesions suggesting that one principle function of lamellipodia is to organize cell-matrix adhesions in a spatially coherent manner.

INTRODUCTION

Cell motility is essential for many biological processes such as embryonic morphogenesis, immune surveillance, and tissue repair. Dysregulation of cell motility is associated with a number of disease states including metastatic cancer and autoimmune disorders (Condeelis et al., 2005; Wickramarachchi et al., 2010). Random motility is thought to allow cells to

[#]Corresponding author: James E. Bear, Lineberger Comprehensive Cancer Center, CB 7295, UNC-Chapel Hill, Chapel Hill, NC 27599-7295 USA, jbear@email.unc.edu, Phone: 919-966-5471, Fax: 919-966-3015.
[*]Equal contributors

effectively sample their environment such as in the case of affinity maturation of B cells in the germinal center (Allen et al., 2007). However, cell migration is frequently governed by various directional cues such as soluble factors (chemotaxis), substrate-attached factors (haptotaxis) or mechanical cues (durotaxis). Understanding how eukaryotic cells sense these directional cues and respond with directed movement remains one of the central problems of modern biology.

Chemotaxis is perhaps the most well understood form of directional motility and involves a variety of signaling pathways connecting cell surface receptors to the motility machinery inside of cells (Swaney et al., 2010). Based mainly on studies of rapidly migrating amoeboid cells such as neutrophils and *Dictyostelium* cells, these signaling cascades are thought to trigger directional protrusions at the leading edge by controlling actin assembly pathways (Parent, 2004). Haptotaxis and durotaxis are much more poorly understood, but likely involve signaling events triggered by adhesive receptors such as integrins (Thiery, 1984).

Fibroblasts are mesenchymal cells that perform a variety of tissue repair functions and respond to directional cues such as gradients of PDGF (Wynn, 2008). In addition, the *in vitro* motility of these cells has been extensively studied. The sheet-like, protruding leading edge of fibroblasts known as the lamellipodium contains a dense array of actin filaments arranged in a dendritic meshwork (Svitkina and Borisy, 1999). Extensive experimental evidence and theoretical models of lamellipodial protrusion indicate that the polymerization of actin filaments within this meshwork drives protrusion (Pollard and Borisy, 2003). In addition to its function in protrusion, the lamellipodium is the site of formation for most cell-matrix adhesions (Webb et al., 2002). Integrin binding to extracellular matrix (ECM) proteins and subsequent clustering lead to the formation of nascent focal complexes appearing continuously at the distal margin of the lamellipodium. A subset of the focal complexes mature into focal adhesions that are connected to bundled actin stress fibers.

The central pillar of the actin network found in lamellipodia is the seven-subunit Arp2/3 complex. The structure, regulation and biochemical properties of this complex have been extensively studied *in vitro* (reviewed in Goley and Welch, 2006). Once activated by nucleation promoting factors (such as SCAR/WAVE), Arp2/3 nucleates actin daughter filaments as branches off of existing mother filaments. The localization of Arp2/3 to actin filament branches *in vivo* (Cai et al., 2008; Svitkina and Borisy, 1999) and the functional role of this complex in lamellipodia formation in cells has been confirmed by many (Nicholson-Dykstra and Higgs, 2008; Rogers et al., 2003; Steffen et al., 2006), but not all studies (Di Nardo et al., 2005). Recently, the existence of actin branches in lamellipodia has been called into question by experiments using alternate electron microscopy techniques (Urban et al., 2010).

Functional studies of Arp2/3 *in vivo* have been severely hampered by effects on viability observed upon loss of this complex in a variety of organisms. Genetic deletion of Arp2/3 subunits is lethal in yeast and *Dictyostelium*, and mouse knockouts produce pre-implantation lethality (Schwob and Martin, 1992; Yae et al., 2006; Zaki et al., 2007). These data led to the prevailing notion that Arp2/3 complex is essential for viability in eukaryotes (Pollard and Cooper, 2009). Here we describe a cell line derived from Ink4a/Arf-deficient mice that can support near complete and stable depletion of Arp2/3 subunits without compromising viability. This cell line has allowed us to directly test the role of Arp2/3 and lamellipodia in fibroblast chemotaxis and haptotaxis.

RESULTS

Development of a stable Arp2/3-depleted cell line

We previously reported a clonal, mouse embryonic fibroblast (MEF) cell line (IA32) derived from an *Ink4a/Arf*−/− animal with unusually prominent lamellipodia (Cai et al., 2008). To develop a stable cell line with fluorescently-tagged Arp2/3 complex in this background, we utilized an established lentiviral shRNA knockdown-rescue (KDR) system to deplete the endogenous p34Arc subunit of the Arp2/3 complex and simultaneously express a GFP-tagged, RNAi-resistant subunit (Vitriol et al., 2007). We separated clonal derivatives of fibroblasts infected with this construct and blotted for p34Arc (Fig. S1A). As expected, we recovered some clones with appropriate depletion and physiological levels of re-expression of the p34Arc-GFP (line 3G6). To our surprise, we also recovered clones that had no re-expression of p34Arc-GFP, but had near complete depletion of the endogenous protein (line 1B3). This result suggested that this cell line, which was derived from an *Ink4a/Arf*−/− mouse (lacking both $p16^{INK4a}$ and Arf), might be able to proliferate in the absence of Arp2/3 complex because of its genetic background. Since Arf is known to play the dominant role in the growth of MEFs (Kamijo et al., 1997), we repeated the depletion of Arp2/3 complex in early passage wild-type (WT) and *Arf*−/− MEFs (lacking Arf only, but retaining $p16^{INK4a}$) and monitored the growth rate. Expression of a non-targeting shRNA (NS) in either background showed no effect on cell proliferation, while depletion of p34Arc (not shown) or the Arp2 subunit strongly reduced the proliferation of WT MEFs, but not *Arf*−/− MEFs (Fig. 1A). These results indicate that in the context of *Ink4a/Arf*−/− or *Arf*−/− MEFs, the Arp2/3 complex is not strictly required for cell viability and that its loss may activate specific growth arrest pathways requiring the Arf tumor suppressor.

Single depletion of either p34Arc or Arp2 in the *Ink4a/Arf*−/− IA32 cell line was not stable over time, and revertant cell lines showing re-expression of the endogenous gene product overwhelmed the culture after 3–5 passages. To produce a more stable Arp2/3 knockdown, we simultaneously depleted both subunits, resulting in a cell line we designated 2xKD (Fig. S1B, C). This cell line showed near complete depletion of both subunits by blotting and concomitant loss of other subunits of the complex as observed by others (Fig. 1B)(Steffen et al., 2006). Quantitative western blotting indicated that depletion levels exceeded 98% (not shown). This depletion was also observed at the single cell level by immunofluorescence (Fig. 1C). Consistent with the growth experiments in early passage MEFs, loss of Arp2/3 complex had no effect on cell proliferation in the IA32 cells (Fig. 1D). Unlike single knockdown cells, these 2xKD cells showed stable depletion of Arp2/3 complex for at least 12 passages. Thus, we employed this system to study the role of Arp2/3 complex in cell motility.

Depletion of Arp2/3 complex leads to the disappearance of lamellipodia and alters actin architecture

Strikingly, despite their normal proliferation rate, the 2xKD cells lost lamellipodia and formed excessive filopodial protrusions (Fig. 1E), consistent with the role of Arp2/3 complex in generating branched actin networks within lamellipodia. To ensure that the lack of lamellipodia was solely due to the absence of Arp2/3 activity, we microinjected bovine Arp2/3 complex into the 2xKD cells, and observed the reappearance of lamellipodia within 20 min after injection (Fig. 1F, Movie 1). This result confirmed the specificity of Arp2/3 depletion and indicated that the upstream activators of Arp2/3 complex were still present and functional in 2xKD cells.

These striking changes in cell morphology prompted us to examine the actin cytoskeleton in the absence of Arp2/3 complex. We first compared F-actin organization in NS and 2xKD

cells by phalloidin staining (Fig. 1C). As expected from the lack of morphological lamellipodia, 2xKD cells have a different pattern of phalloidin staining with no areas of enrichment in peripheral regions. We also utilized electron microscopy (EM) to investigate leading edge actin networks in detail. A recently described method involving rapid freezing, freeze-drying and high-resolution metal shadowcasting developed for visualizing purified protein complexes (Ozgur et al., 2011) was extended to the imaging of cells plated directly on EM grids. The spreading and formation of protrusions was confirmed by live-cell imaging of the grids in pilot experiments (not shown). This method allowed us to prepare the cells without critical point drying and replica formation. We observed drastically different actin filament architectures at the margins of 2xKD cells compared to the NS control cells (Fig. 1G). The NS cells had a network of short, interconnected filaments with many examples of branching. This architecture is similar to the networks observed with platinum replica EM previously (Svitkina and Borisy, 1999). The 2xKD cells had a much more sparse network of longer filaments that were highly bundled which frequently converged into higher order bundles in filopodia. Actin filament crosslinks and some end-to-side junctions could be observed in the 2xKD cells, suggesting multiple forms of crosslinking and bundling still occur in the absence of the Arp2/3 complex. Overall, our results are consistent with the obligate role of Arp2/3 complex in generating densely branched actin networks.

Arp2/3-depleted cells show inefficient, filopodia-driven cell motility

Since lamellipodia are thought to play important roles in cell migration, we examined the effect of Arp2/3 depletion and loss of lamellipodia on cell motility using single cell tracking. 2xKD cells and cells singly depleted of either p34Arc or Arp2 showed a marked reduction in migration speed compared to NS cells. The reduced speed was fully rescued in both p34-KDR and Arp2-KDR cells re-expressing RNAi resistant p34Arc or Arp2 subunits respectively, as well as doubly depleted and doubly rescued (2KDR) cells (Fig. 2A), confirming that neither of the effects of the respective shRNAs was due to off-target effects. A similar reduction of cell migration speed was observed when NS cells were treated with the Arp2/3 inhibitor CK-666 (100 μM), but not with the inactive compound CK-689 (Nolen et al., 2009). This same concentration of the Arp2/3 inhibitor did not affect cell speed or morphology of 2xKD cells (Fig. 2B, not shown), confirming the near complete depletion of Arp2/3 complex and suggesting that the residual motility in 2xKD cells was not dependent on any remaining Arp2/3 complex activity. To test whether the residual motility in 2xKD cells was still dependent on actin assembly, we treated cells with latrunculin B (LatB) to inhibit F-actin polymerization. Both NS and 2xKD cells showed significant reduction in cell speed when F-actin polymerization was impaired (Fig. 2C), suggesting that the Arp2/3-depleted cells still rely on actin assembly to migrate.

One possible mechanism by which the 2xKD cells could continue to migrate, albeit slowly, is by relying on myosin contractility. To address this, we treated cells with blebbistatin (BLB), a myosin II inhibitor. This treatment decreased focal adhesion and stress fiber staining, but increased phosphorylation of the myosin light chain at Ser19 (Fig. S2A–C), consistent with previous studies (Goeckeler et al., 2008). Based on this previous work, increased phospho-myosin light chain does not reflect an increase in cellular contractility in this case. In the motility assay, BLB treatment increased 2xKD cell speed significantly without an effect on the speed of NS cells (Fig. 2D). This result indicates that the residual motility of the Arp2/3-depleted cells does not depend on myosin contractility. We observed from time-lapse DIC images (not shown) and F-actin staining (Sup. Fig. S2A) that BLB treatment increased filopodia number in 2xKD cells. Filopodia were counted in NS and 2xKD cells treated with BLB or DMSO control using scanning electron microscopy (SEM) (Fig. 2E). Control 2xKD cells have approximately three-fold more filopodia than NS cells.

Filopodia number in BLB-treated 2xKD cells increased significantly while the number of filopodia remained unchanged in BLB-treated NS cells (Fig. 2F). Time-lapse imaging revealed that 2xKD cells create new areas of flat protrusion by “filling the gap” between adjacent filopodia (Movie 2). Occasionally, the tips of two adjacent filopodia fuse and the resulting hole fills in (Movie 2). Due to the larger number of filopodia on the BLB-treated 2xKD cells, more of these “filling the gap” events were observed (Fig. 2G), correlating with higher whole cell motility. Together, these observations suggest that cells have an alternate, filopodia-driven form of protrusion in the absence of Arp2/3 activity which leads to relatively inefficient whole cell translocation.

Chemotaxis in the absence of Arp2/3 complex

Loss of Arp2/3 complex causes changes in leading edge actin organization and disappearance of lamellipodia, leading to reduced random cell motility. However, cell migration speed and the ability to respond to directional cues are independent properties and rigorous experimental approaches are required to separately measure these properties. To address this issue, we utilized a modified version of a previously described microfluidic chemotaxis chamber (Fig. 3A; (Shamloo et al., 2008)) which allowed us to directly image the migration of cells exposed to a defined gradient of chemoattractant for >12 hrs. The establishment and maintenance of a linear soluble gradient in this device was confirmed using fluorescent dextran (Fig. 3B) Based on the fluorescence intensity profile, this equates to a slope of 43.6 %/mm across the cell culture chamber. The average cell in our experiments was ~150 μm across in the dimension of the gradient which yields a chemoattractant slope of ~6.5% across an individual cell. In every experiment, NS expressing GFP and 2xKD cells were seeded in the same cell culture chamber and serum starved prior to establishment of the PDGF gradient. DIC live-cell imaging was used to monitor cell movement, and gradient stability was monitored at each time point by imaging the gradient of Cy5-dextran for up to 16 hr (Movie 3).

Single cell tracking was used to follow individual cells over time and calculate the velocity and directionality of migration. We utilized two methods to calculate the directional bias of the resulting tracks. First, we transposed the tracks so that each had its start point at the origin and then computed the forward migration index (FMI) using the final position of the cell at the end of the track (Fig. 3C). Second, we calculated the angle of each turn in the track relative to the gradient and plotted these as a histogram (Fig. 3D). Using this distribution of turn angles, we used a non-linear curve fit to compute the compass parameter (CP) as described previously (Arrieumerlou and Meyer, 2005). Surprisingly, no statistically significant difference in either FMI or CP was observed between NS and 2xKD cells at all source concentrations of PDGF tested (Fig. 3E, S3A). In experiments with early passage single knockdown cells (p34-KD) and knockdown-rescue cells (p34-KDR), we used serum as a more generic chemoattractant and observed the same result (Fig. S3B). This result was further confirmed using Rat2 fibroblasts treated with the Arp2/3 complex inhibitor CK-666. As with the Arp2/3-depleted IA32 cells, inhibition of Arp2/3 activity had no effect on the ability to respond to the PDGF gradient (Fig. 3F, S3C). These results indicate that although Arp2/3 and lamellipodia play important roles in increasing the efficiency of cell migration, they are not essential for directional sensing of chemotactic gradients in fibroblasts.

To confirm that proximal signaling events in the PDGF pathway were also unaffected by Arp2/3 depletion, levels of total and phosphorylated Akt (pAkt) in response to PDGF stimulation were examined by blotting. Similar changes in Akt signaling were observed in 2xKD and NS cells upon PDGF stimulation (Fig. 3G). Since 2xKD cells can respond to gradients of PDGF, we examined the morphological response of these cells to acute, uniform stimulation with PDGF. While NS cells produced lamellipodia and ruffles (Fig. S3D), 2xKD cell increased the number of filopodia (Fig. 3H, Movie 4). We also examined

2xKD cells during chemotaxis up a PDGF gradient and observed that these cells had more filopodia on the up-gradient side of the cell (Fig. 3I). Together, these results indicate that PDGF signaling is intact in the absence of Arp2/3 complex, but that cells produce filopodia in response to this stimulus rather than lamellipodia without Arp2/3.

Depletion of Arp2/3 leads to defects in cell spreading

When cells encounter surfaces coated with extracellular matrix proteins, they initiate a spreading process that involves the dynamic reorganization of the actin cytoskeleton. To examine spreading in the absence of Arp2/3 complex, we plated NS and 2xKD cells expressing GFP-Paxillin (GFP-Pax) on fibronectin (FN)-coated surfaces and stained cells at different time-points for F-actin and phospho-tyrosine (pTyr). The 2xKD cells showed a marked delay in spreading kinetics and the expected absence of peripheral lamellipodia (Fig. 4A, B). Both pTyr and GFP-Pax showed focal adhesions had formed in the 2xKD cells by 90 min, but most of these adhesions remained associated with the periphery compared with the NS controls. To quantify the cell-spreading defect, we used an impedance-based system that measures electrical changes caused by cells interacting with a microelectrode within the surface of a dish. Arp2/3-depleted cells showed statistically significant decrease in cell spreading compared to control cells (Fig. 4C). Consistent with the delay in physical spreading, the 2xKD cells showed delayed and reduced adhesion signaling during spreading as reported by the phosphorylation of Focal Adhesion Kinase (FAK) at Tyr397 (Fig. 4D).

Arp2/3 and lamellipodia are essential for responding to absolute or gradient changes in ECM concentration

Although spreading provides useful information about the initial formation of cell-matrix adhesions, changes in the motility of fully spread cells in response to changes in matrix concentration are more physiologically relevant. Many investigators have noted that cells display a biphasic motility response when plated on different concentrations of ECM with optimal motility occurring at intermediate concentrations (DiMilla et al., 1993; Gupton and Waterman-Storer, 2006). We tested the role of Arp2/3 and lamellipodia in this biphasic motility response. As expected, when plated on different concentrations of FN, NS cells displayed a biphasic motility response. However, 2xKD cells migrated at a constant, slow speed on all FN concentrations tested (Fig. 5A). This result was confirmed with Rat2 fibroblasts treated with the Arp2/3 inhibitor CK-666 (Fig. 5B). This loss of biphasic motility response led us to explore the role of Arp2/3 complex and lamellipodia in haptotaxis.

Using the same microfluidic system as in the chemotaxis experiments, we were able to establish a linear ECM gradient bound to the surface of the cell culture chamber prior to plating the cells (Fig. 5C). The chamber was thoroughly flushed prior to plating the cells to ensure that no soluble FN remained that could act as a chemoattractant. As in the chemotaxis experiments, NS and 2xKD cells were plated in the same device for live cell imaging during haptotaxis. We plotted endpoint positions and angular turn per step based on cell tracking data and found that both measurements showed a dramatic difference between NS and 2xKD cells (Fig. 5D,E; Movie 5). Haptotactic FMI and CP of 2xKD cells showed that these cells have no directional response to concentration gradients of FN, despite a robust haptotactic response of NS cells plated in the same chamber. This result was the same with all source concentrations of FN tested (Fig. 5F, S4A). In addition to FN, we tested other ECM proteins (laminin (LN) and vitronectin (VTN)) that utilize different integrin receptors and observed that 2xKD cells show complete absence of haptotaxis on all ECMs tested (Fig. 5G, S4A). Finally, we confirmed this result with Rat2 fibroblasts treated with the Arp2/3 inhibitor CK-666 and observed that Arp2/3 activity was required for haptotaxis in this cell line (Fig. 5H, S4B). Together, these results reveal an essential role of Arp2/3

complex and lamellipodia in responding to changes in either the absolute concentration or gradient presentation of ECM.

Depletion of Arp2/3 complex leads to altered focal adhesion morphology and dynamics

The defects in the ability to sense and/or respond to changes in ECM observed in the 2xKD cells suggest that cell-matrix interactions may be changed when Arp2/3 complex and lamellipodia are absent. To address this question, we compared the distribution of focal adhesion proteins by immunofluorescence. Endogenous Paxillin (Pax), Vinculin (Vin) and FAK were all present at clearly recognizable focal adhesions in 2xKD cells (red asterisks, Fig. 6A), although there were no obvious focal complexes present in these cells due to the lack of lamellipodia. To visualize the dynamics of focal adhesions, GFP-Pax was expressed in NS and 2xKD cells. Using TIRF microscopy, we observed that both cell types contained GFP-Pax positive focal adhesions, but that these two cell types tended to form adhesions in qualitatively different ways. In line with descriptions from other cell types, the NS cells generated small focal complexes at the distal margin of lamellipodia, a subset of which matured into focal adhesions. These adhesions matured in the distal to proximal direction (Fig. 6B). In the 2xKD cells, however, the focal adhesions first appeared at the base of filopodia and reached maximal intensity quite rapidly (within 1–2 min, Fig. 6C). Unlike in the NS cells, these adhesions grow in the proximal to distal direction. These qualitative differences in the formation of focal adhesions suggested that cells depleted of Arp2/3 complex were utilizing alternative pathways of adhesion assembly.

To quantify the parameters of the individual focal adhesions once formed in both cell types, we used a recently developed method to segment and track every focal adhesion in an unbiased manner (Fig. S5A–D)(Berginski et al., 2011). We analyzed the focal adhesion properties of NS and 2xKD cells across three concentrations of fibronectin (Fig. 6D). With increasing fibronectin concentration, mean focal adhesion area and mean longevity were increased in the NS cells. Interestingly, neither of these properties varies significantly in the 2xKD cells as a function of fibronectin concentration. Mean long axis length and mean axial ratio are the same in both cell types and do not vary with fibronectin concentration. The number of adhesions per cell (per 10 min) trends in the opposite direction in NS and 2xKD cells as a function of fibronectin concentration. Control NS cells have decreased numbers of adhesions per cell with increasing fibronectin, while Arp2/3-depleted 2xKD cells have increased numbers of adhesions with increasing fibronectin concentration. We also examined the focal adhesions in Rat2 fibroblasts expressing GFP-Pax treated with the Arp2/3 inhibitor CK-666 or its inactive analogue CK-689. With transient Arp2/3 inhibition, some of the same trends in focal adhesion properties were evident (and statistically significant), but were much less pronounced than with RNAi-based depletion. Together these data indicate that some focal adhesion properties are unchanged by Arp2/3 depletion, while others are altered when Arp2/3 is depleted.

Lamellipodia promote global focal adhesion alignment

Although the characterization of individual focal adhesion parameters is important, the ensemble pattern of adhesions is the most relevant parameter to whole cell behavior. How cells control these ensemble or global parameters of focal adhesions is poorly understood. We observed that during spreading and after cells had fully spread, 2xKD cells had adhesions that were more radially arrayed and less aligned to each other than the NS cells (Fig. 6A). One possible way adhesions could become aligned to each other is through rotation of their long axis. Although our visual impression from TIRF movies of cells expressing GFP-Pax strongly argued against this possibility, we tested this by plotting the average deviation in long-axis angle during the time that an individual adhesion was observed. Consistent with our visual impression, focal adhesions show very little variation

in their long-axis angle over time in either cell type (Fig. 7A). Thus, any change in global alignment must arise from spatially coherent formation, rather than post-formation realignment.

To quantify global focal adhesion alignment, we developed a method to measure the deviation of adhesion angles from the most frequent or dominant angle observed in the whole cell (see Fig S6). In order to reliably determine the angle of the individual adhesions, we limited our measurements to those adhesions with a length/width ratio of at least 3 (Fig. 7B). By plotting the angles of all the adhesions that met this criterion, we were able to determine the most frequent or dominant focal adhesion angle by rotating the image frame of reference until the standard deviation (SD) was minimized and the peak of the distribution of angles moved close to zero (Fig. S6B). The dominant focal adhesion angle was simply the degree to which the image had to be rotated to center the peak over zero. The Focal Adhesion Alignment Index (FAAI) is directly related to the standard deviation of this distribution; FAAI = 90-SD in order to have a higher index value correspond to more aligned adhesions (Fig. 7C). To illustrate this measurement, a cell with high FAAI and low FAAI are shown in Fig. 7D (Movie 6).

Using this metric, we quantified the FAAI of NS and 2xKD cells plated on 1, 10 and 100 μg/mL fibronectin. We observed increased alignment of adhesions across the cell (increasing FAAI) with increasing fibronectin concentration in the NS cells, while the alignment in the 2xKD cells was decreased compared to the NS cells and was constant at all fibronectin concentrations (Fig. 7E). Since mean adhesion area showed similar trends (Fig. 6D), we tested whether focal adhesion alignment was independent from adhesion area. To do this, we re-calculated the FAAI considering only small, medium or large adhesions in the NS and 2xKD cells (Fig. 7F). Regardless of which size adhesions we used to calculate FAAI, the same difference in alignment was observed between NS and 2xKD cells. To ensure that this result was not specific to the expression of GFP-Pax, we calculated the FAAI of NS and 2xKD cells expressing fluorescent fusions of FAK and Vinculin. With all three markers, 2xKD cells showed significantly lower FAAI compared to NS control cells (Fig. 7G). Finally, we confirmed this result in Rat2 fibroblasts treated with the Arp2/3 complex inhibitor CK-666 where we observed decreased FAAI with Arp2/3 inhibition (Fig. 7H). These results suggest that one of the principal functions of the lamellipodium is to promote global focal adhesion alignment.

DISCUSSION

In this work, we have established a stable Arp2/3-depleted cell line that allowed us to study random and directional cell motility in the absence of lamellipodia. The depletion of Arp2/3 complex causes striking changes in cell morphology, motility and global focal adhesion geometry. Furthermore our study also reveals the essential role of lamellipodia in fibroblast haptotaxis, but not chemotaxis.

Establishment of a stable Arp2/3 depleted cell line

It is widely believed that Arp2/3 complex is required for viability in eukaryotic organisms, however our data suggest that this is not strictly true in mammalian cells in culture. It is worth considering why we were able to recover stable cell lines depleted of >98% of Arp2/3 complex. First, we quickly separated the cells as clones after they were infected with the shRNA-expressing lentiviruses through the use of fluorescent protein reporters rather than relying on drug resistance. Any selective growth advantage conferred by less than full knockdown is cancelled out under these circumstances. Although we initially had some concerns about using clones, these were put to rest by the microinjection rescue experiment that indicated that these cells were still capable of making lamellipodia within minutes of the

re-introduction of the Arp2/3 complex. Second, we depleted two essential subunits (p34Arc and Arp2) to create a "fail-safe" condition where loss of either shRNA conferred no advantage due to the continued absence of another essential subunit. Third, the complexity of mammalian cells may have been working in our favor. Simpler eukaryotes may be strictly dependent on Arp2/3 activity for viability-associated processes such as nutrient uptake, while mammalian cells have a multitude of partially redundant pathways. Finally, we performed these experiments in the *Ink4a/Arf*-deficient background. These genes are well known as tumor suppressors that arrest cell growth upon oncogenic insult (Kim and Sharpless, 2006). Our results indicate that cells harboring an intact Arf gene are much more sensitive to the loss of Arp2/3 complex, suggesting that the deranged actin cytoskeleton resulting from the loss of Arp2/3 activity may trigger an Arf-dependent growth arrest pathway.

The relationship between Arp2/3 complex and lamellipodia

The most striking morphological change we observed in the Arp2/3 complex depleted cells was the disappearance of lamellipodia. We report several lines of evidence to support the idea that the phenotypic loss of lamellipodia is due to a specific loss of Arp2/3 complex activity. Both shRNAs used to deplete p34Arc and Arp2 respectively could be fully rescued by co-expression of RNAi-resistant versions of these genes. Pharmacological inhibition of Arp2/3 complex by CK-666 produced a similar, although slightly milder phenotype as the double depletion of p34Arc and Arp2. Importantly, this compound had no further effect on the 2xKD cells, indicating that any residual Arp2/3 activity was not contributing to the residual motility. Furthermore, lamellipodia could be recovered in the 2xKD cells within minutes of microinjection of bovine Arp2/3 complex. Therefore, the 2xKD cells are not only useful in the study of Arp2/3 complex dependent functions, but also serve as useful tools to dissect the functional role of lamellipodia in cell motility.

Previous studies have shown that the actin networks within lamellipodia contain short, branched filaments nucleated by Arp2/3 complex (Svitkina and Borisy, 1999), consistent with observations of networks generated with purified Arp2/3 complex and actin (Mullins et al., 1998). Recently, this model has been called into question based on an alternate electron microscopy protocol (Urban et al., 2010). Using this technique, mostly long actin filaments were observed in the lamellipodia. Our results with the cryo-shadowing technique are entirely consistent with the notion of highly branched networks of short actin filaments in lamellipodia as originally observed by platinum replica EM (Svitkina and Borisy, 1999). Further evidence for the role of Arp2/3 complex in branch generation comes from the apparent lack of these structures in cells with near total depletion of Arp2/3 complex.

In the absence of branched actin generated by the Arp2/3 complex, more filopodial protrusions form on the periphery of cells. 2xKD cells engage in a form of filopodia-dependent cell motility, in which new flat cell surface area is created by "filling the gap" between adjacent filopodia. The filopodia of 2xKD cells protrude and bend until they become anchored to the underlying matrix, at which time the membrane between two filopodia gradually fills-in. When myosin II was inhibited in the 2xKD cells using blebbistatin, we observed increased filopodia number and "filling the gap" behavior, and a proportional increase in cell speed. This suggests that the Arp2/3 depleted cells rely on this filopodia-initiated "filling the gap" motility to migrate. This form of motility is relatively inefficient compared to motility using lamellipodia; however, efficiency of motility does not necessarily relate to the ability of cells to sense or respond to directional cues.

The role of lamellipodia in chemotaxis

Chemotaxis is required for numerous physiological processes and has been the subject of intense study for well over a century. The most successful model systems have been the social amoeba *Dictyostelium* and amoeboid cells of the haematopoietic system such as neutrophils (Parent, 2004). Studies of chemotaxis in amoeboid cells and other cell types have largely focused on the signal transduction cascades that connect cell surface receptors to the polymerization of actin at the protrusive leading edge. As lamellipodia are the actin-rich, protrusive organelle in fibroblasts, we fully anticipated that depletion of Arp2/3 complex and the resulting loss of lamellipodia would have a profound impact on fibroblast chemotaxis. To our surprise, depletion of Arp2/3 complex has no effect whatsoever on fibroblast chemotaxis up shallow gradients of PDGF, other than affecting the speed at which the cells crawl. Although stimulated actin assembly may still be important for chemotactic response, this assembly clearly does not involve the Arp2/3 complex in this cell type. However, other forms of actin assembly such as those that lead to the increased filopodia on the 2xKD cells may be important for chemotaxis. It is also worth noting that our results may not translate to amoeboid cell chemotaxis, which may require Arp2/3 activity. Future studies will focus on testing the role of alternate actin assembly pathways in fibroblast chemotaxis and testing the generality of our findings for other cell types.

Although the normal chemotaxis of Arp2/3-depleted fibroblasts is surprising, several studies point toward a more complex picture of chemotaxis than previously appreciated. Transient depletion of either the Cdc42 or Rac1 small GTPase or both does not affect the ability of fibroblasts to respond to gradients of PDGF (Monypenny et al., 2009). Similar to our cells, these depletions affect the morphology of the leading edge without affecting chemotaxis, although some non-GTPase dependent activation of Arp2/3 cannot be excluded. Another enzyme that was initially thought to be crucial for chemotaxis, PI-3 Kinase, is also not strictly required for chemotaxis of *Dictyostelium* amoebae based on genetic studies (Hoeller and Kay, 2007) or fibroblast chemotaxis towards PDGF based on pharmacological inhibition of this enzyme (Melvin et al., 2011). Together with our results, these studies highlight the complexity of chemotactic mechanisms and the insufficiency of current models in explaining this process.

The role of lamellipodia in sensing/responding to changes in ECM

Our results with the Arp2/3 depleted cells reveal the importance of Arp2/3 complex and lamellipodia in sensing and responding to the changes in the ECM. Several groups have reported that cells exhibit a biphasic motility response to variable extracellular matrix concentration with fast migration occurring at intermediate ECM concentration and slower migration occurring at low and high ECM concentrations (DiMilla et al., 1993; Gupton and Waterman-Storer, 2006). The molecular basis of this biphasic response is thought to involve spatiotemporal feedback between actomyosin and focal adhesion systems (Gupton and Waterman-Storer, 2006); however, the relationship between this response and specific cellular architecture is unclear. Our data indicate that Arp2/3 and lamellipodia are required for the biphasic response of cells to variable ECM. Stated another way, the adhesions formed by the filopodial protrusions on the 2xKD cells are insufficient to allow cells to sense or respond to these differences in ECM concentration. This suggests that the adhesions formed within lamellipodia have qualitatively different properties that allow the whole cell to coordinate global motility.

Cells not only can regulate velocity when migrating on different concentrations of ECM, but also can sense and respond to ECM gradients and migrate in a directional way. This process, termed haptotaxis, requires cells to 1) sense differences of ECM concentration/engagment across a single cell, 2) polarize cytoskeletal and motility machinery, and 3) migrate up the

gradient. Our data show that Arp2/3 depletion and subsequent loss of lamellipodia completely ablates haptotaxis. Importantly, this was true not only on gradients of fibronectin, but also on gradients of laminin or vitronectin, ECMs that require different integrin heterodimers. One outstanding question about the role of lamellipodia in haptotaxis is whether this structure is involved in sensing the gradient or responding to the gradient or both. Considering the intact PDGF chemotactic response without Arp2/3 complex, the loss of haptotaxis appears to be a specific effect rather than a general defect in direction sensing. This remarkable difference in the need for lamellipodia between chemotaxis and haptotaxis suggests that cells use very different mechanisms to sense and respond to these different directional cues.

Spatial organization of cell-matrix adhesions and global cell motility

Although focal adhesions have been intensively studied for decades, the processes that spatially organize these structures in an ensemble manner across the whole cell are poorly understood. Our results indicate that lamellipodia play a major role in bringing spatial coherence to focal adhesion formation. Without lamellipodia, focal adhesions are poorly aligned to each other, which may explain why these cells migrate slowly. An open question is how lamellipodia promote the alignment of focal adhesions. One possibility is that the retrograde flow of actin networks in lamellipodia, which is itself spatially coherent over 0.5–5 μm length scales, could promote the alignment of the adhesions that form and mature within this flow field. However, how the alignment of focal adhesions within lamellipodia contribute to global alignment is less clear. Since the rear of the cell was once the front the cell, this alignment may reflect the history of these adhesions as born within previous lamellipodia. How cells manage to define a new axis of focal adhesion alignment upon turning will be the subject of future studies.

Our observations also provide a conceptual framework for linking events occurring at small length scales such as the formation of branches by the Arp2/3 complex (~10 nm) to whole cell motility at much longer length scales (~100 μm) (Fig. 7I). Branched actin networks generated by the Arp2/3 complex are the main component of the lamellipodial cytoskeleton. As we have shown in this paper, lamellipodia are critical for the alignment of focal adhesions. Cells with aligned focal adhesions will have aligned stress fibers attached to those adhesions. Since stress fibers are the main contractile structure of fibroblasts, cells with aligned focal adhesions will have more coherent contractility. We postulate that this coherent contractility will contribute directly to efficient whole cell migration. This overall notion is consistent with our observation that a strong relationship exists between the fibronectin concentration the cells are plated on, the global alignment of focal adhesions, and their increased cell speed. Future studies will focus on testing this hypothesis in context of other 2D and 3D motility events.

EXPERIMENTAL PROCEDURES

Cell culture, viral transduction and generation of 2xKD cells

Cells were cultured in DMEM supplemented with 10% FBS (HyClone), 100 U/mL pen/strep and 292 μg/mL L-glutamine. DMEM supplemented with 0.1% fatty-acid free BSA (Equitech-Bio) was used to culture cells during serum starvation. Lentivirus production and infection were as described (Cai et al., 2007). IA32 cells infected with viruses were cloned by fluorescence-activated cell-sorting (FACS) and screened for p34 and Arp2 expression by blotting. For complete methods, see Extended Experimental Procedures in Supplemental Material section.

Microscopy and image analysis

For immunofluorescent staining, the cells were fixed, stained and mounted as described previously (Bear et al., 2002). Primary antibodies were applied to cells in PBS containing 1% BSA as indicated in Extended Experimental procedures. For live-cell imaging, cells were plated on 10 μg/mL FN-coated glass bottom culture dishes (MatTek Corporation) for 8–12 hr before imaging. Time-lapse microscopy was performed on an Olympus VivaView FL microscope or with Nikon BioStation IM. Cell speed was measured with ImageJ using the Manual Tracking plug-in (http://rsbweb.nih.gov/ij/plugins/track/track.html). Total internal reflectance microscopy was performed using Olympus cell^TIRF illuminator motorized multicolor TIRF microscope. Electron microscopy was performed as described in Extended Experimental Procedures.

Directional migration assays

PDMS-based microfluidic devices were fabricated as described in the Extended Experimental Procedures. For chemotaxis assays, the source syringe was filled serum free DMEM containing indicated chemoattractant and 10 μg/mL of TRITC-dextran to visualize the gradient. The sink syringe contained only serum free DMEM. The syringe pump was operated at a flow rate of 20 nL/min. A stable gradient was established in the cell culture chamber within 30 min, and typically remained stable for 18 hr as monitored by TRITC-dextran fluorescent intensity. For haptotaxis assays, the cell culture was coated with a minimal concentration of 2.5 μg/mL FN (or 5 μg/mL LN) to promote cell attachment throughout the chamber. The source and sink syringes were filled with the indicated concentration FN (or LN or VTN) in PBS or PBS alone respectively. The syringe pump was maintained at a flow rate of 20 nL/min. The chambers were allowed to equilibrate for 1 hr. Once the ECM gradient was established on the surface, 1 mg/mL PLL(20)-g[3.5]-PEG(2) was flowed into all channels of the device to block non-specific adhesion. Thorough wash of the chambers with distilled water was performed before plating the cells. Imaging for directional migration assays was performed and analyzed as described in Extended Experimental Procedures section.

Focal Adhesion Segmentation and Measurements

To identify focal adhesions in each image of a time-lapse series, a set of segmentation methods were used (Berginski et al., 2011). In order to measure the global alignment of focal adhesions across the entire cell, we developed the focal adhesion alignment index (FAAI, Figure S5A, B). A complete description of these procedures is contained in the Extended Experimental Procedures section.

Supplementary Material

Refer to Web version on PubMed Central for supplementary material.

Acknowledgments

We gratefully acknowledge support from HHMI, NIH grants to JEB (GM083035), NES (UO1-CA141576), SMG (DK037871) and JDG (GM31819, ES 13773), the LCCC Electron Microscopy Core (supported by NIH CA16086) the UNC-Olympus Imaging Research Center, UNC Research Computing, the Allbrittion lab for use of facilities, members of the Bear lab for critical discussions, Zenon Rajfur for assistance with microinjection, and Klaus Hahn for the mCherry-FAK construct.

REFERENCES

Allen CD, Okada T, Tang HL, Cyster JG. Imaging of germinal center selection events during affinity maturation. Science. 2007; 315:528–531. [PubMed: 17185562]

Arrieumerlou C, Meyer T. A local coupling model and compass parameter for eukaryotic chemotaxis. Developmental cell. 2005; 8:215–227. [PubMed: 15691763]

Bear JE, Svitkina TM, Krause M, Schafer DA, Loureiro JJ, Strasser GA, Maly IV, Chaga OY, Cooper JA, Borisy GG, et al. Antagonism between Ena/VASP Proteins and Actin Filament Capping Regulates Fibroblast Motility. Cell. 2002; 109:509–521. [PubMed: 12086607]

Berginski ME, Vitriol EA, Hahn KM, Gomez SM. High-resolution quantification of focal adhesion spatiotemporal dynamics in living cells. PLoS ONE. 2011; 6:e22025. [PubMed: 21779367]

Cai L, Makhov AM, Schafer DA, Bear JE. Coronin 1B antagonizes cortactin and remodels Arp2/3-containing actin branches in lamellipodia. Cell. 2008; 134:828–842. [PubMed: 18775315]

Cai L, Marshall TW, Uetrecht AC, Schafer DA, Bear JE. Coronin 1B coordinates Arp2/3 complex and cofilin activities at the leading edge. Cell. 2007; 128:915–929. [PubMed: 17350576]

Condeelis J, Singer RH, Segall JE. The great escape: when cancer cells hijack the genes for chemotaxis and motility. Annual review of cell and developmental biology. 2005; 21:695–718.

Di Nardo A, Cicchetti G, Falet H, Hartwig JH, Stossel TP, Kwiatkowski DJ. Arp2/3 complex-deficient mouse fibroblasts are viable and have normal leading-edge actin structure and function. Proceedings of the National Academy of Sciences of the United States of America. 2005; 102:16263–16268. [PubMed: 16254049]

DiMilla PA, Stone JA, Quinn JA, Albelda SM, Lauffenburger DA. Maximal migration of human smooth muscle cells on fibronectin and type IV collagen occurs at an intermediate attachment strength. J Cell Biol. 1993; 122:729–737. [PubMed: 8335696]

Goeckeler ZM, Bridgman PC, Wysolmerski RB. Nonmuscle myosin II is responsible for maintaining endothelial cell basal tone and stress fiber integrity. American journal of physiology Cell physiology. 2008; 295:C994–C1006. [PubMed: 18701651]

Goley ED, Welch MD. The ARP2/3 complex: an actin nucleator comes of age. Nature reviews Molecular cell biology. 2006; 7:713–726.

Gupton SL, Waterman-Storer CM. Spatiotemporal feedback between actomyosin and focal-adhesion systems optimizes rapid cell migration. Cell. 2006; 125:1361–1374. [PubMed: 16814721]

Hoeller O, Kay RR. Chemotaxis in the absence of PIP3 gradients. Current biology : CB. 2007; 17:813–817. [PubMed: 17462897]

Kamijo T, Zindy F, Roussel MF, Quelle DE, Downing JR, Ashmun RA, Grosveld G, Sherr CJ. Tumor suppression at the mouse INK4a locus mediated by the alternative reading frame product p19ARF. Cell. 1997; 91:649–659. [PubMed: 9393858]

Kim WY, Sharpless NE. The regulation of INK4/ARF in cancer and aging. Cell. 2006; 127:265–275. [PubMed: 17055429]

Melvin AT, Welf ES, Wang Y, Irvine DJ, Haugh JM. In chemotaxing fibroblasts, both high-fidelity and weakly biased cell movements track the localization of PI3K signaling. Biophysical journal. 2011; 100:1893–1901. [PubMed: 21504725]

Monypenny J, Zicha D, Higashida C, Oceguera-Yanez F, Narumiya S, Watanabe N. Cdc42 and Rac family GTPases regulate mode and speed but not direction of primary fibroblast migration during platelet-derived growth factor-dependent chemotaxis. Molecular and cellular biology. 2009; 29:2730–2747. [PubMed: 19273601]

Mullins R, Heuser J, Pollard T. The interaction of Arp2/3 complex with actin: nucleation, high affinity pointed end capping, and formation of branching networks of filaments. Proc Natl Acad Sci U S A. 1998; 95:6181–6186. [PubMed: 9600938]

Nicholson-Dykstra SM, Higgs HN. Arp2 depletion inhibits sheet-like protrusions but not linear protrusions of fibroblasts and lymphocytes. Cell motility and the cytoskeleton. 2008; 65:904–922. [PubMed: 18720401]

Nolen BJ, Tomasevic N, Russell A, Pierce DW, Jia Z, McCormick CD, Hartman J, Sakowicz R, Pollard TD. Characterization of two classes of small molecule inhibitors of Arp2/3 complex. Nature. 2009; 460:1031–1034. [PubMed: 19648907]

Ozgur S, Damania B, Griffith J. The Kaposi's sarcoma-associated herpesvirus ORF6 DNA binding protein forms long DNA-free helical protein filaments. Journal of structural biology. 2011; 174:37–43. [PubMed: 21047556]

Parent CA. Making all the right moves: chemotaxis in neutrophils and Dictyostelium. Current opinion in cell biology. 2004; 16:4–13. [PubMed: 15037299]

Pollard T, Borisy G. Cellular motility driven by assembly and disassembly of actin filaments. Cell. 2003; 112:453–465. [PubMed: 12600310]

Pollard TD, Cooper JA. Actin, a central player in cell shape and movement. Science. 2009; 326:1208–1212. [PubMed: 19965462]

Rogers SL, Wiedemann U, Stuurman N, Vale RD. Molecular requirements for actin-based lamella formation in Drosophila S2 cells. J Cell Biol. 2003; 162:1079–1088. [PubMed: 12975351]

Schwob E, Martin RP. New yeast actin-like gene required late in the cell cycle. Nature. 1992; 355:179–182. [PubMed: 1729653]

Shamloo A, Ma N, Poo MM, Sohn LL, Heilshorn SC. Endothelial cell polarization and chemotaxis in a microfluidic device. Lab Chip. 2008; 8:1292–1299. [PubMed: 18651071]

Steffen A, Faix J, Resch GP, Linkner J, Wehland J, Small JV, Rottner K, Stradal TE. Filopodia formation in the absence of functional WAVE- and Arp2/3- complexes. Molecular biology of the cell. 2006; 17:2581–2591. [PubMed: 16597702]

Svitkina TM, Borisy GG. Arp2/3 complex and actin depolymerizing factor/cofilin in dendritic organization and treadmilling of actin filament array in lamellipodia. The Journal of cell biology. 1999; 145:1009–1026. [PubMed: 10352018]

Swaney KF, Huang CH, Devreotes PN. Eukaryotic chemotaxis: a network of signaling pathways controls motility, directional sensing, and polarity. Annu Rev Biophys. 2010; 39:265–289. [PubMed: 20192768]

Thiery JP. Mechanisms of cell migration in the vertebrate embryo. Cell Differ. 1984; 15:1–15. [PubMed: 6394144]

Urban E, Jacob S, Nemethova M, Resch GP, Small JV. Electron tomography reveals unbranched networks of actin filaments in lamellipodia. Nature cell biology. 2010; 12:429–435.

Vitriol EA, Uetrecht AC, Shen F, Jacobson K, Bear JE. Enhanced EGFP-chromophore-assisted laser inactivation using deficient cells rescued with functional EGFP-fusion proteins. Proc Natl Acad Sci U S A. 2007; 104:6702–6707. [PubMed: 17420475]

Webb DJ, Parsons JT, Horwitz AF. Adhesion assembly, disassembly and turnover in migrating cells -- over and over and over again. Nature cell biology. 2002; 4:E97–E100.

Wickramarachchi DC, Theofilopoulos AN, Kono DH. Immune pathology associated with altered actin cytoskeleton regulation. Autoimmunity. 2010; 43:64–75. [PubMed: 20001423]

Wynn TA. Cellular and molecular mechanisms of fibrosis. The Journal of pathology. 2008; 214:199–210. [PubMed: 18161745]

Yae K, Keng VW, Koike M, Yusa K, Kouno M, Uno Y, Kondoh G, Gotow T, Uchiyama Y, Horie K, et al. Sleeping beauty transposon-based phenotypic analysis of mice: lack of Arpc3 results in defective trophoblast outgrowth. Mol Cell Biol. 2006; 26:6185–6196. [PubMed: 16880528]

Zaki M, King J, Futterer K, Insall RH. Replacement of the essential Dictyostelium Arp2 gene by its Entamoeba homologue using parasexual genetics. BMC genetics. 2007; 8:28. [PubMed: 17553170]

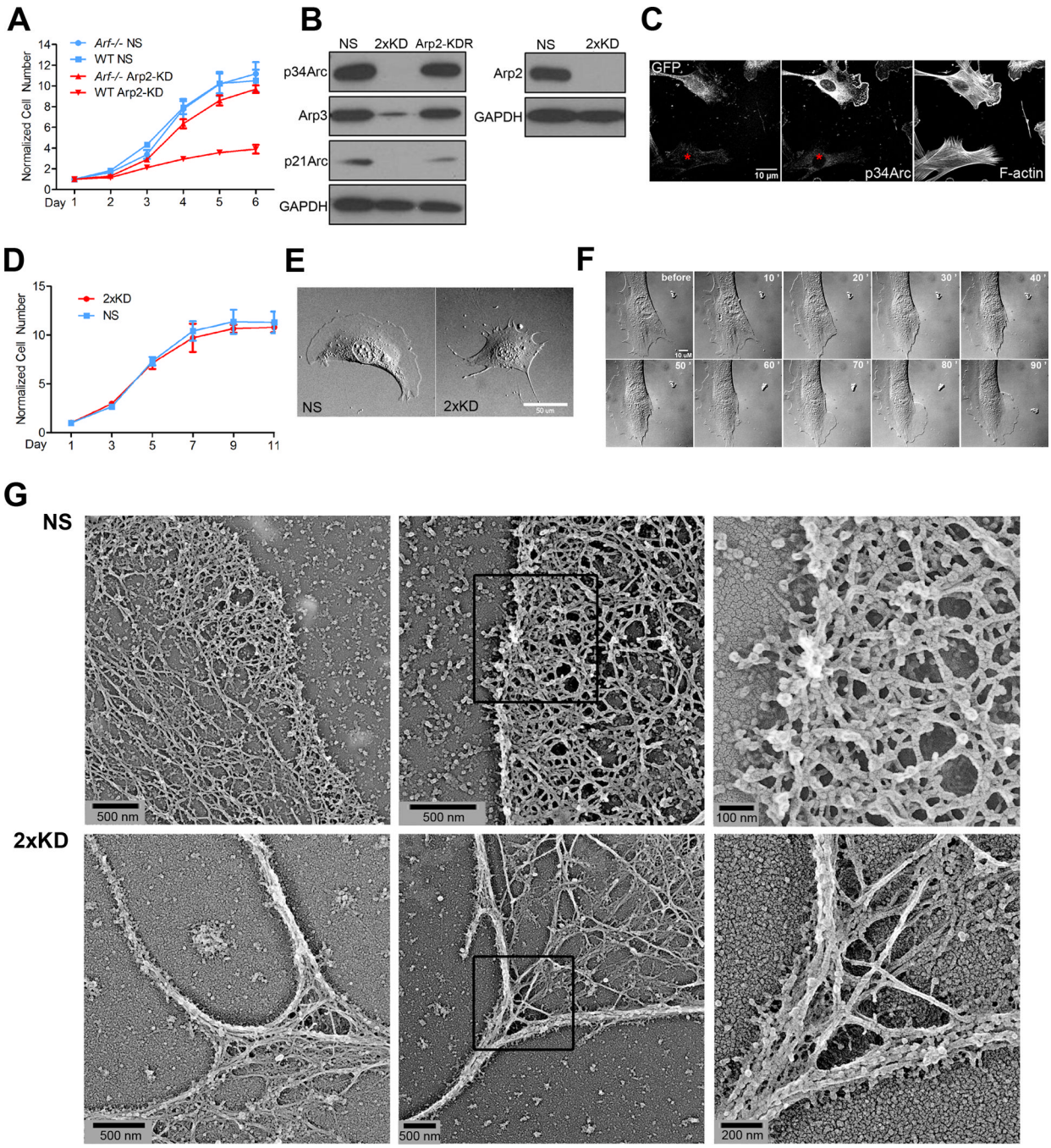

Figure 1. Establishment of a stable Arp2/3 complex depleted cell line

1A) Growth curve of wild-type (WT) and *Arf* −/− early passage MEFs infected with lentivirus expressing a non-specific sequence (NS) shRNA or Arp2 shRNA (Arp2-KD). Error bars: SEM

1B) IA32 cells were infected with lentivirus that expressed shRNAs against NS, p34Arc and Arp2 (2xKD), or shArp2 that also co-expressed human Arp2-GFP (Arp2-KDR). Lysates were blotted for p34Arc, Arp3, p21Arc, Arp2 and for GAPDH as a loading control

1C) Mixed NS (expressing GFP) and 2xKD cells (marked by red asterisks) were immunostained for p34Arc to verify knockdown of the endogenous gene and phalloidin to visualize F-actin. Also see Fig. 1D,E

1D) Growth curve of NS and 2xKD cells. Error bars: SEM
1E) DIC images of NS and 2xKD cells (Scale bar: 50 μm)
1F) 2xKD cells were microinjected with 5 mg/mL Arp2/3 complex. Representative time-lapse sequence before and after injection show the reappearance of lamellipodia. See movie 1
1G) Cryo-shadowing EM images showing the leading edge actin networks of NS and 2xKD cells. Left and middle panels are separate cells, right panel is magnified portion of middle panels indicated by black boxes
See also Fig. S1 and Movie 1

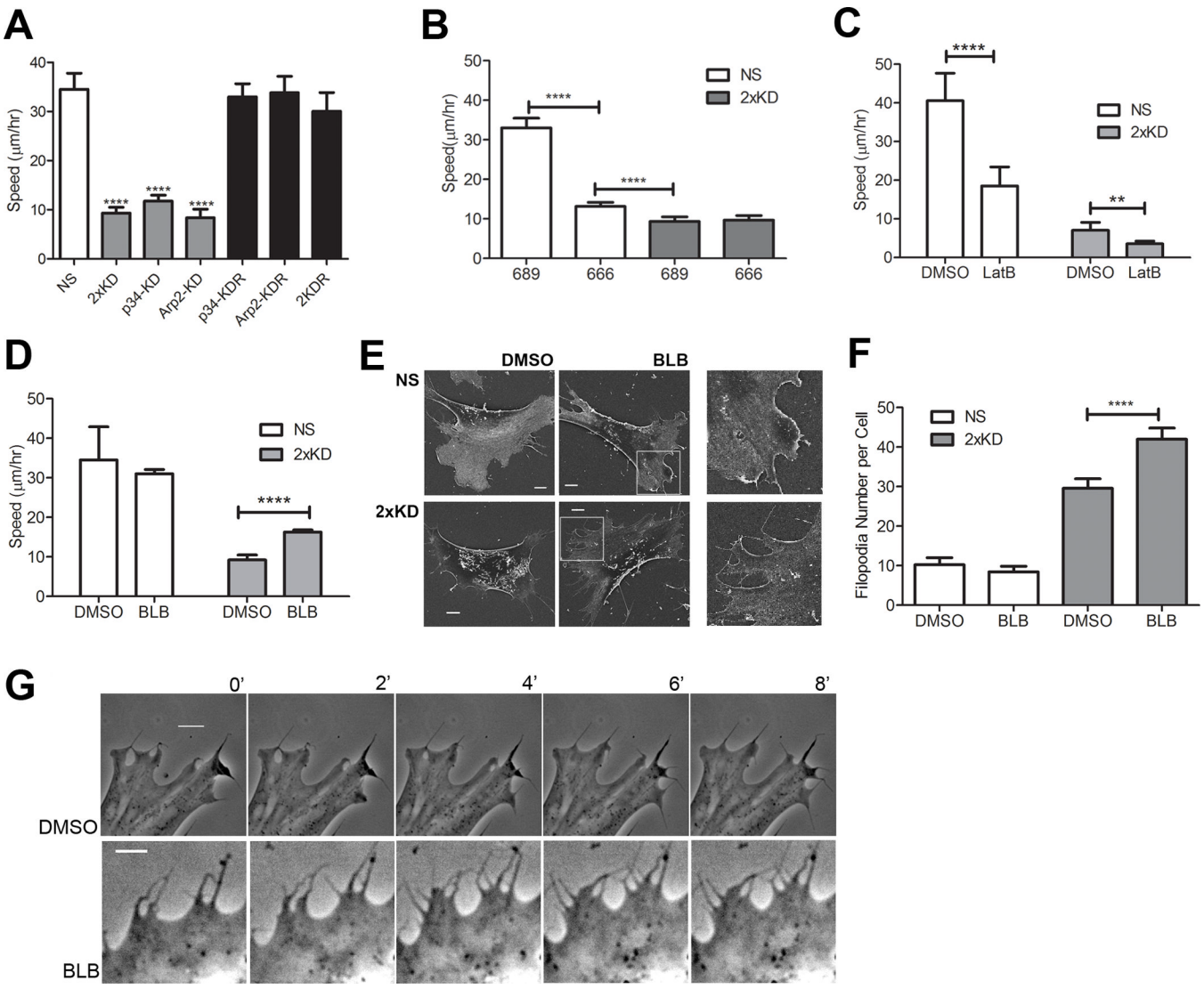

Figure 2. Arp2/3-depleted cells show inefficient, filopodia-driven cell motility

2A) Time-lapse microscopy of NS, 2xKD, p34-KD Arp2-KD, p34-KDR and Arp2-KDR and 2KDR cell lines was used to determine single-cell speed, depicted in graph. Error bars represent 95% confidence intervals. ****P<0.0001 by Student's t-test

2B) Single-cell speed of NS and 2xKD cells treated with 100 μM Arp2/3 inhibitor CK-666 or the inactive control compound CK-689. Error bars represent 95% confidence intervals. ****P<0.0001 by Student's t-test

2C) Single-cell speed of NS and 2xKD cells treated with 1μM Latrunculin B (LatB) or DMSO as a control. Error bars represent 95% confidence intervals. ****P<0.0001, **P<0.01 by Student's t-test

2D) Single-cell speed of NS and 2xKD cells treated with 15 μM blebbistatin (BLB) or DMSO as a control. Error bars represent 95% confidence intervals. ****P<0.0001 by Student's t-test

2E) SEM images of NS and 2xKD cells treated with DMSO or BLB

2F) Number of filopodia/cell with DMSO or BLB treatment was calculated from >30 cells in each cell line from SEM images. ****P<0.0001 by Student's t-test

2G) Time-lapse images of 2xKD cells treated with DMSO or BLB. Scale bar: 5 μm

See also Fig. S2 and Movie 2

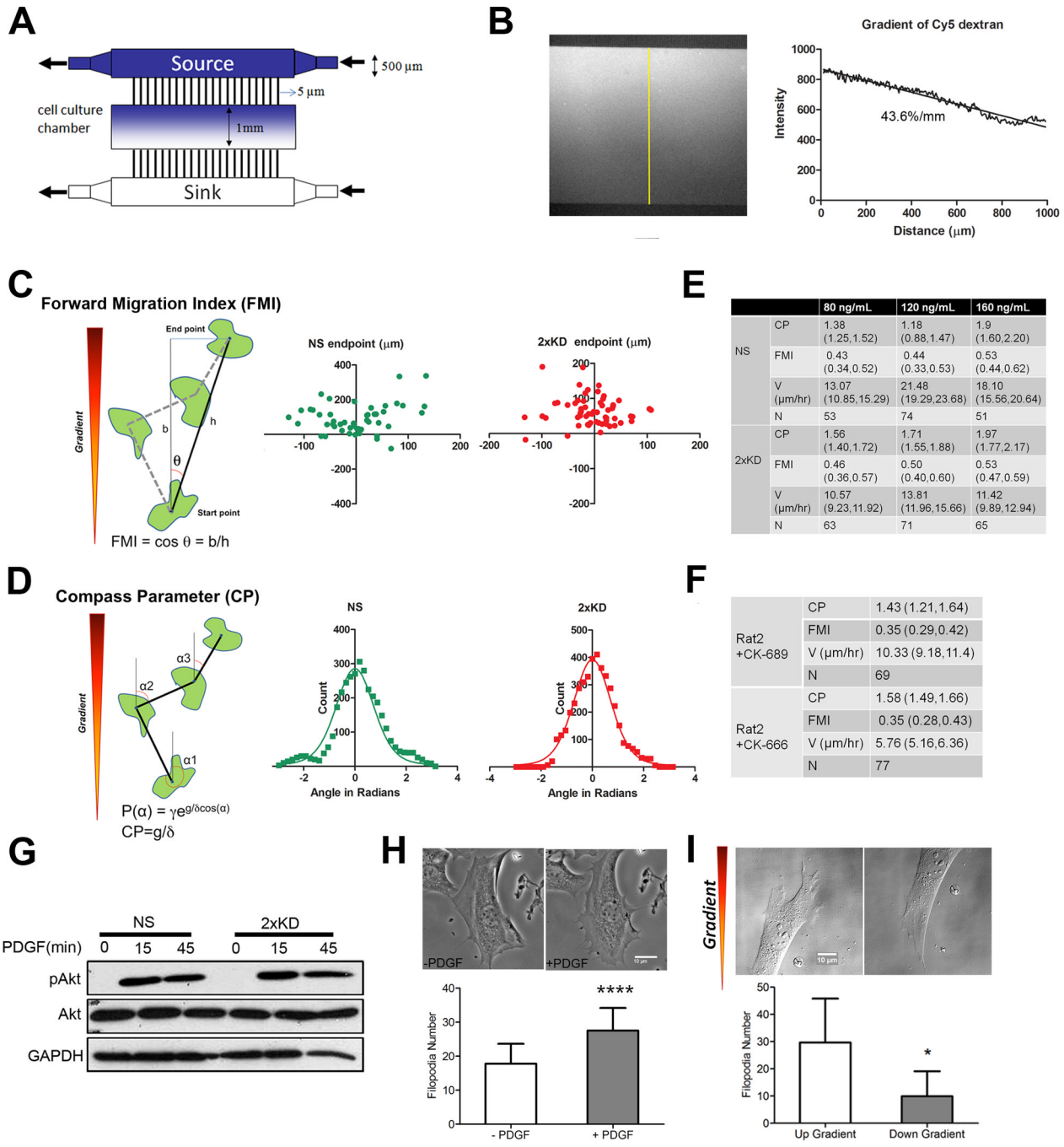

		80 ng/mL	120 ng/mL	160 ng/mL
NS	CP	1.38 (1.25,1.52)	1.18 (0.88,1.47)	1.9 (1.60,2.20)
	FMI	0.43 (0.34,0.52)	0.44 (0.33,0.53)	0.53 (0.44,0.62)
	V (μm/hr)	13.07 (10.85,15.29)	21.48 (19.29,23.68)	18.10 (15.56,20.64)
	N	53	74	51
2xKD	CP	1.56 (1.40,1.72)	1.71 (1.55,1.88)	1.97 (1.77,2.17)
	FMI	0.46 (0.36,0.57)	0.50 (0.40,0.60)	0.53 (0.47,0.59)
	V (μm/hr)	10.57 (9.23,11.92)	13.81 (11.96,15.66)	11.42 (9.89,12.94)
	N	63	71	65

Rat2 +CK-689	CP	1.43 (1.21,1.64)
	FMI	0.35 (0.29,0.42)
	V (μm/hr)	10.33 (9.18,11.4)
	N	69
Rat2 +CK-666	CP	1.58 (1.49,1.66)
	FMI	0.35 (0.28,0.43)
	V (μm/hr)	5.76 (5.16,6.36)
	N	77

Figure 3. Arp2/3 complex depletion does not affect chemotaxis

3A) Schematic of the microfluidic chamber for chemotaxis and haptotaxis experiments

3B) Left: fluorescent image of Cy5-dextran gradient formed inside the chamber as an indication of gradient formation and maintenance. Right: line-scan plot of the gradient along the yellow line depicted in the left panel, slope of the gradient is indicated under the curve

3C) Diagram showing FMI calculation method and representative end point scatter plots of NS and 2xKD cells in chemotaxis assays (Data from 120 ng/mL source PDGF concentration)

3D) Diagram showing Compass Parameter (CP) calculation and representative histograms showing angular turn per step of NS and 2xKD cells in the same PDGF chemotaxis assays

as in 3C. P(α) is the probably distribution of angles measured relative to gradient, γ is a constant, g is the gradient steepness and δ is the angular step size (Arrieumerlou and Meyer, 2005)

3E) Table showing compass parameter (CP), forward migration index (FMI), velocity (V) and number of cells analyzed (N) in chemotaxis assays with indicated PDGF source concentrations. Numbers in parentheses for each entry are 95% confidence intervals

3F) Table showing Rat2 cell chemotaxis parameters in the presence of Arp2/3 inhibitor CK-666 or its inactive control CK-689

3G) Western blotting showing the change of phospho-Akt (pAkt) level upon PDGF stimulation. Cells were serum-starved overnight before stimulation with 40 ng/mL PDGF

3H) 2xKD cells before and after PDGF stimulation (images) and the number of filopodia before and after PDGF treatment of 2xKD cells was calculated from >30 2xKD cells. *P<0.05 by Student's t-test

3I) Example of the filopodia up and down the PDGF gradient in 2xKD cell chemotaxis was shown and the number of filopodia was calculated from >30 2xKD cells. *P<0.001 by Student's t-test

See also Fig. S3 and Movies 3 and 4

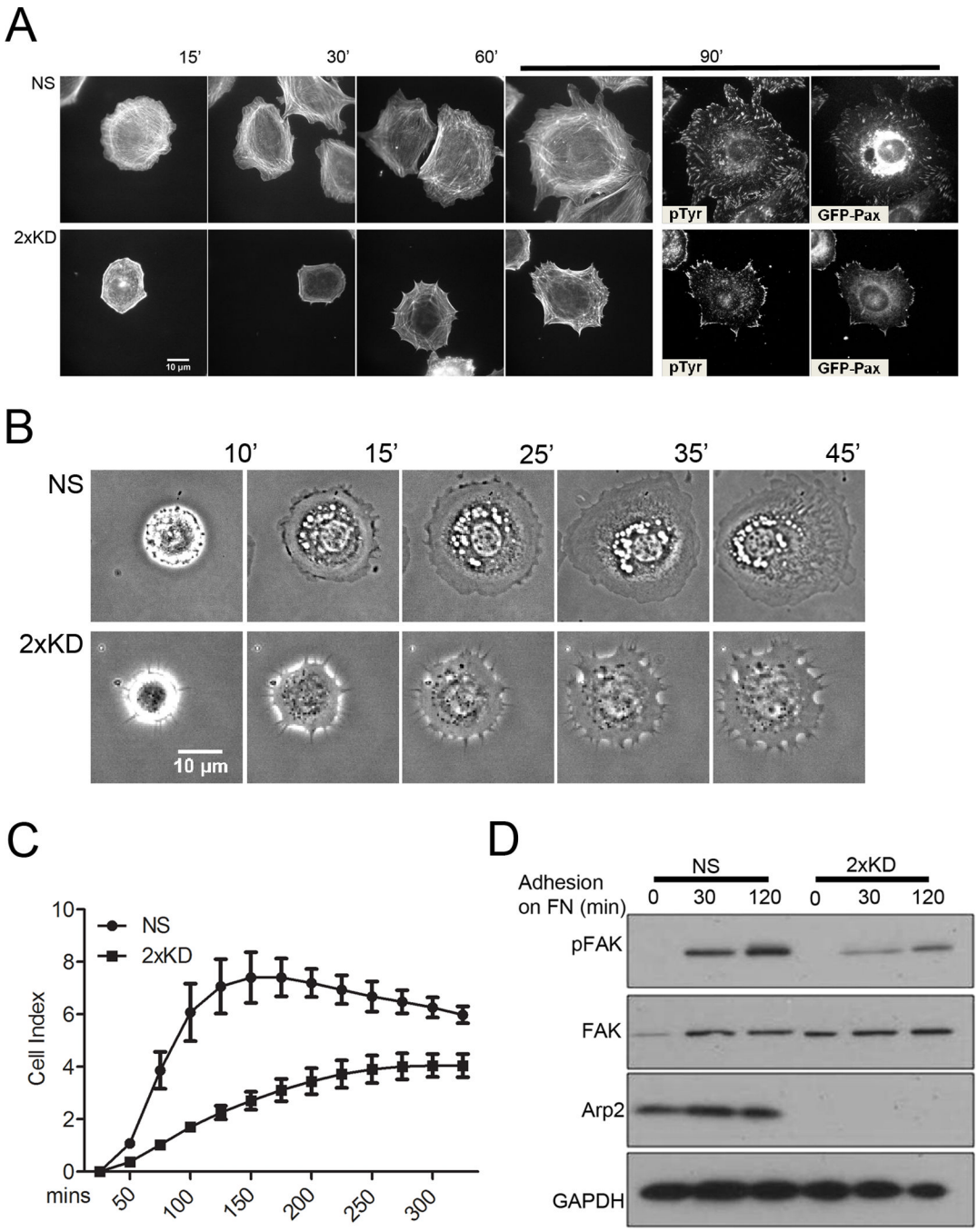

Figure 4. Arp2/3 depletion inhibits cell spreading

4A) NS and 2xKD cells expressing GFP-Pax were immunostained for phospho-tyrosin (pTyr) and F-actin at different time points during cell spreading

4B) Time-lapse images showing the spreading of NS and 2xKD cells

4C) Cell adhesion and spreading kinetics of NS and 2xKD cells were analyzed using an impedance based system and reported as arbitrary units (Cell Index). Error bars: SEM

4D) Western blotting showing the change of phosphorylated FAK (pFAK) level upon cell adhesion to fibronectin. Cells were serum-starved overnight and trypsinized and plated on fibronectin-coated surface. Lysates were blotted for pFAK, total FAK, Arp2 and GAPDH as control

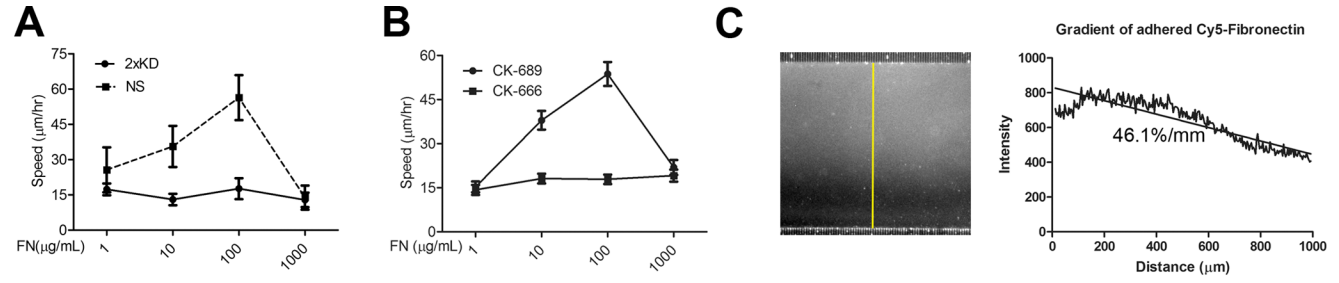

F

		100 μg/mL FN	250 μg/mL FN	500 μg/mL FN
NS	CP	0.67 (0.57,0.78)	1.3 (1.11,1.50)	1.00 (0.86,1.15)
	FMI	0.16 (0.06,0.26)	0.38 (0.32,0.44)	0.23 (0.14,0.31)
	V (μm/hr)	15.20 (14.24,16.16)	22.56 (21.11,24.01)	14.91 (14.09,15.73)
	N	50	100	60
2xKD	CP	0.14 (0.07,0.21)	-0.04 (-0.11,0.04)	0.02 (-0.09,0.13)
	FMI	0.03 (-0.04,0.11)	0.0006 (-0.08,0.08)	0.02 (-0.08,0.12)
	V (μm/hr)	21.59 (20.36,22.82)	17.88 (15.53,20.23)	17.24 (16.21,18.27)
	N	53	85	57

G

		250 μg/mL FN	500μg/mL LN	100 μg/mL VTN
NS	CP	1.3 (1.11,1.50)	1.63 (1.43,1.83)	1.00 (0.71,1.3)
	FMI	0.38 (0.32,0.44)	0.26 (0.21,0.30)	0.30 (0.23,0.38)
	V (μm/hr)	22.56 (21.11,24.01)	22.85 (21.43,24.3)	21.36 (19.82,22.91)
	N	100	84	46
2xKD	CP	-0.04 (-0.11,0.04)	0.15 (-0.02,0.31)	-0.09 (-0.18,0.001)
	FMI	0.0006 (-0.08,0.08)	0.01 (-0.04,0.07)	-0.04 (-0.13,0.05)
	V (μm/hr)	17.88 (15.53,20.23)	15.95 (14.9,17.9)	15.56 (14.48,16.64)
	N	85	54	43

H

Rat2 +CK-689	CP	1.23 (0.96,1.52)
	FMI	0.30 (0.25,0.36)
	V (μm/hr)	23.46 (21.3,25.62)
	N	109
Rat2 +CK-666	CP	0.15 (0.02,0.27)
	FMI	-0.01 (-0.05,0.03)
	V (μm/hr)	20.0 (18.23,21.73)
	N	121

Figure 5. Arp2/3 complex depleted cells cannot respond to concentration or gradient changes in extracellular matrix

5A) Single-cell speed of NS and 2xKD cells plated on different concentrations of fibronectin was plotted (N>30). Error bars represent 95% confidence intervals

5B) Speeds of Rat2 cells treated with CK-666 or CK-689 and plated on different concentrations of FN were plotted (N>30). Error bars represent 95% confidence intervals

5C) Left: fluorescent image of Cy5-fibronectin gradient formed on the glass surface inside the cell culture chamber. Right: line-scan plot of the gradient along the yellow line depicted in the left panel

5D) Representative end point scatter plots of NS and 2xKD cells in haptotaxis assays (250 μg/mL source fibronectin concentration)

5E) Representative histogram showing angular turn per step of NS and 2xKD cells in the same haptotaxis assays as in 5D

5F) Table showing compass parameter (CP), forward migration index (FMI), velocity (V) and number of cells analyzed (N) in haptotaxis assays with indicated FN source concentrations. Numbers in parentheses for each entry are 95% confidence intervals

5G) Table showing compass parameter (CP), forward migration index (FMI), velocity (V) and number of cells analyzed (N) in haptotaxis assays with indicated extracellular matrix

5H) Table showing compass parameter (CP), forward migration index (FMI), velocity (V) and number of cells analyzed (N) in Rat2 cell haptotaxis assays with 250 μg/mL source fibronectin concentration and treated with CK-666 or CK-689

See also Fig. S4 and Movie 5

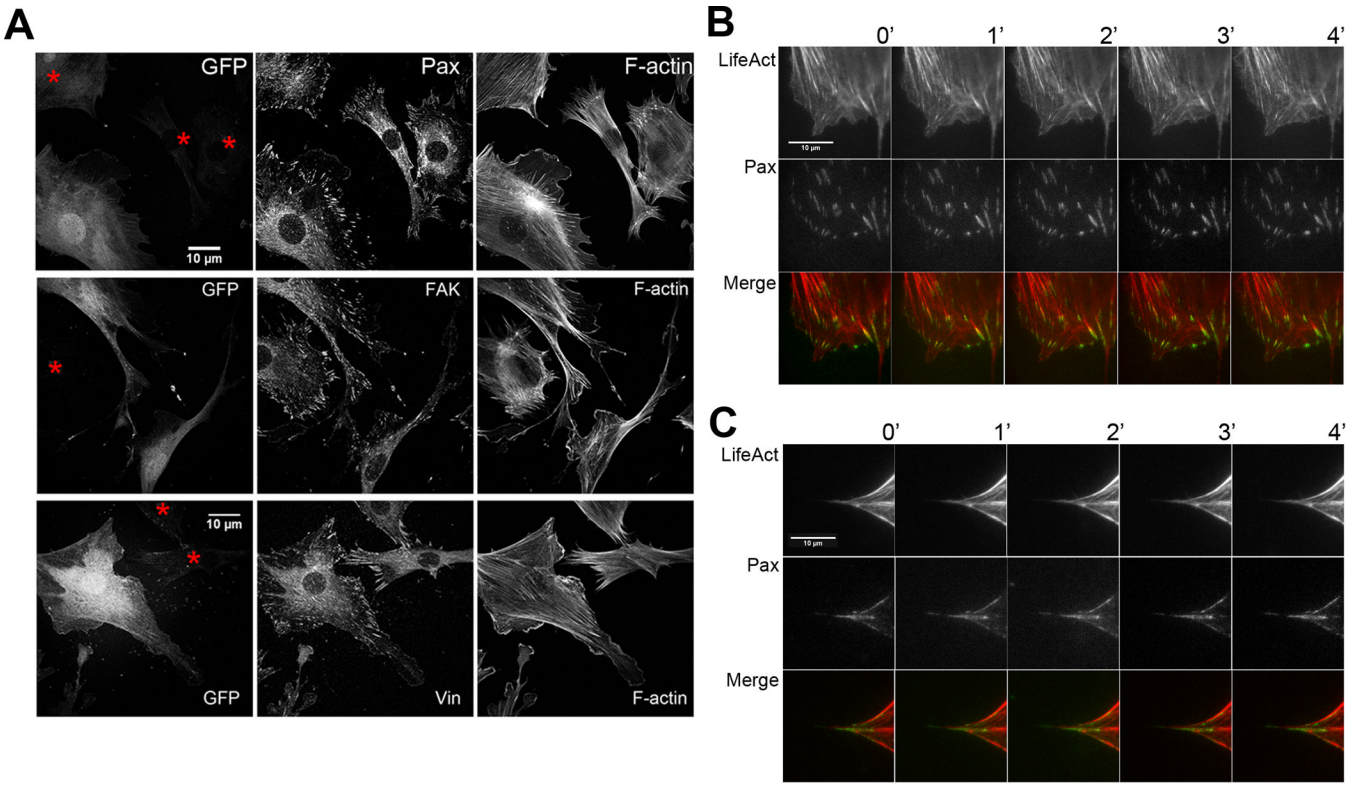

D

		Mean Area (μm²)	Mean Axial Ratio	Mean Major Axis (μm)	Mean Minor Axis (μm)	Mean Longevity (min)	Adhesions/Cell/10 min	# Adhesions	# Cells
NS	1 μg/mL FN	0.057±0.00031	2.0±0.0015	0.4±0.0007	0.2±0.0004	4.4±0.03	728.0±193.0	169735	25
	10 μg/mL FN	0.065±0.00081	2.0±0.0022	0.4±0.0013	0.2±0.0007	4.9±0.05	431.5±124.0	80552	16
	100 μg/mL FN	0.082±0.00107	1.9±0.0034	0.4±0.0020	0.2±0.0010	6.1±0.09	262.6±79.3	49154	17
2xKD	1 μg/mL FN	0.054±0.00037	2.0±0.0023	0.4±0.0008	0.2±0.0005	4.5±0.04	286.6±95.9	77917	21
	10 μg/mL FN	0.056±0.00049	2.0±0.0026	0.4±0.0010	0.2±0.0006	4.6±0.04	324.6±152.1	63260	15
	100 μg/mL FN	0.053±0.00019	2.0±0.0012	0.4±0.0004	0.2±0.0003	4.4±0.02	802.5±161.7	254105	22
Rat2	CK-689	0.057±0.00053	1.9±0.0031	0.4±0.0012	0.2±0.0007	4.7±0.07	303.1±124.1	42576	12
	CK-666	0.054±0.00048	1.9±0.0021	0.4±0.0008	0.2±0.0005	4.4±0.04	305.0±147.5	77942	20

Figure 6. Depletion of Arp2/3 complex leads to defective focal adhesion morphology and dynamics

6A) Mixed NS (expressing GFP) and 2xKD cells (marked by red asterisks) were immunostained for endogenous paxillin (Pax), focal adhesion kinase (FAK), vinculin (Vin) and F-actin (Scale bar: 10 μm).

6B) Representative time-lapse TIRF images of an NS cell expressing GFP-Pax and LifeAct-tagRFP

6C) Representative time-lapse TIRF images of a 2xKD cell expressing GFP-Pax and LifeAct-tagRFP

6D) Table of focal adhesion parameters: NS vs 2xKD plated on 1, 10 and 100 μg/mL FN; Rat2 fibroblasts treated with CK-666 or CK-689 on 100 μg/mL FN. Numbers after the +/− indicate 95% confidence intervals as determined by a t-distribution fit

See also Fig. S5

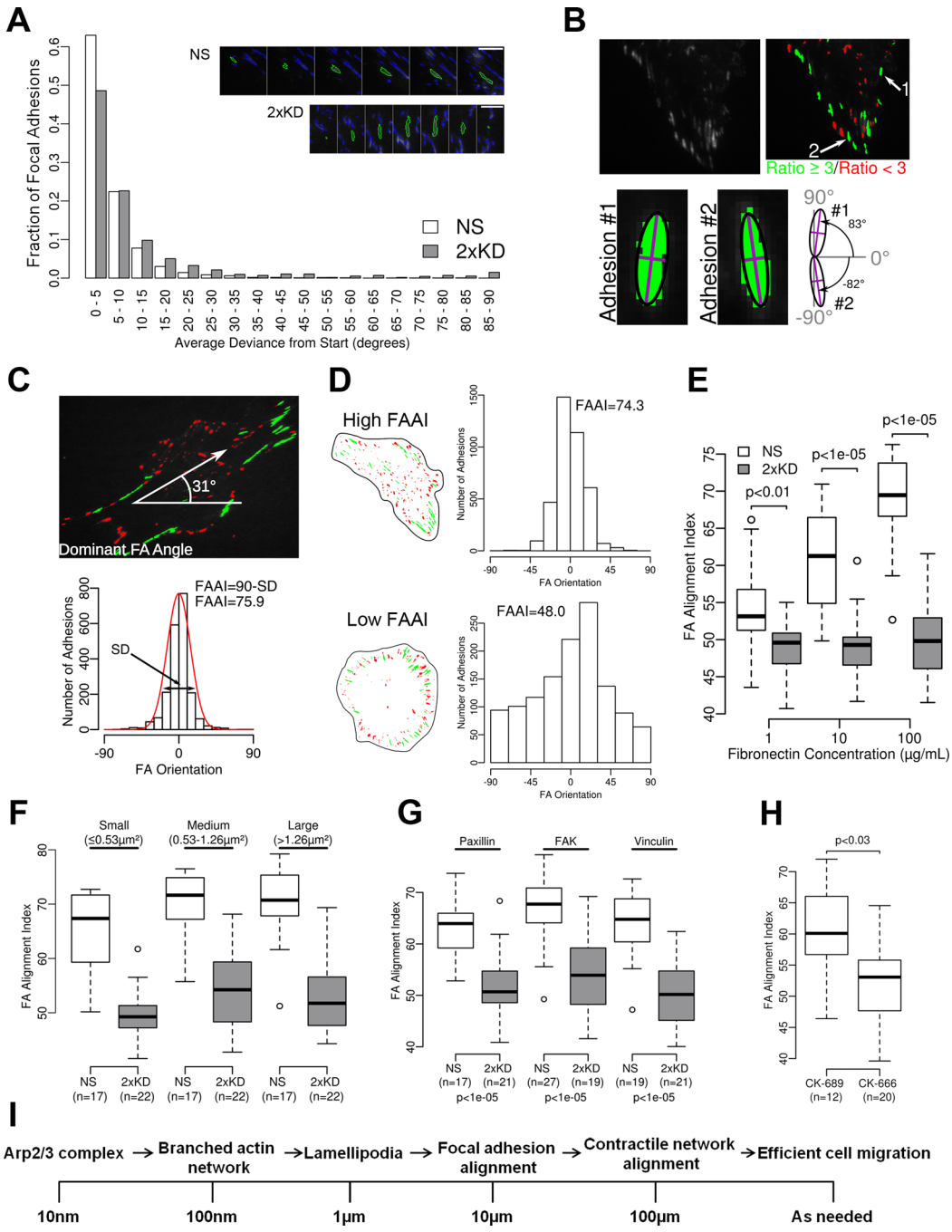

Figure 7. Arp2/3 complex depletion leads to poor global alignment of focal adhesions

7A) Distribution of single focal adhesion mean deviations from their first orientation measurement starting point. The adhesions analyzed were from NS (17 cells and 3184 adhesions) or 2xKD (22 cells and 1132 adhesions) cells plated on 100 µg/mL fibronectin. Insets show single adhesions outlined in green through time, there are 6 minutes between each image

7B) Diagram showing adhesion filtering through a minimum axial ratio of 3 and two sample adhesion orientations

7C) Diagram showing the determination of dominant angle and focal adhesion alignment index (FAAI)

7D) Sample single cell cartoons showing representative high and low FAAI cells with corresponding adhesion orientation data sets
7E) FAAI of NS and 2xKD cells expressing GFP-Paxillin plated on different concentrations of fibronectin (number of cells same as in Fig. 6D, p-values for the difference between the means were calculated by bootstrapping with 10000 replicates)
7F) FAAI of NS and 2xKD cells with the adhesions grouped by size (p-values for each size range <0.0005)
7G) FAAI of NS and 2xKD cells expressing indicated focal adhesion markers. (n = number of cells analyzed, p-values calculated same as in 7E)
7H) FAAI of Rat2 cells with CK-666 or CK-689
7I) Conceptual model of cell motility events across length scales
See also Fig. S6 and Movie 6